Water Resources Research

RESEARCH ARTICLE
10.1029/2019WR025310

A Precipitation Recycling Network to Assess Freshwater Vulnerability: Challenging the Watershed Convention

J. Keune[1] and D. G. Miralles[1]

[1]Laboratory of Hydrology and Water Management, Ghent University, Ghent, Belgium

Key Points:
- From 9% and up to 74% of summer precipitation over European watersheds is supplied by other European watersheds
- A watershed precipitation recycling network illustrates the dependencies and key suppliers of freshwater for Europe during summer
- The strong interdependence of watersheds through precipitation recycling highlights the need of global water governance

Supporting Information:
- Supporting Information S1

Correspondence to:
J. Keune,
jessica.keune@ugent.be

Citation:
Keune, J., & Miralles, D. G. (2019). A precipitation recycling network to assess freshwater vulnerability: Challenging the watershed convention. *Water Resources Research*, *55*, 9947–9961. https://doi.org/10.1029/2019WR025310

Received 5 APR 2019
Accepted 18 OCT 2019
Accepted article online 10 NOV 2019
Published online 28 NOV 2019

Abstract Water resources and water scarcity are usually regarded as local aspects for which a watershed-based management appears adequate. However, precipitation, as a main source of freshwater, may depend on moisture supplied through land evaporation from outside the watershed. This notion of evaporation as a local "green water" supply to precipitation is typically not considered in hydrological water assessments. Here we propose the concept of a *watershed precipitation recycling network*, which establishes atmospheric pathways and links land surface evaporation as a moisture supply to precipitation, hence contributing to local but also remote freshwater resources. Our results show that up to 74% of summer precipitation over European watersheds depends on moisture supplied from other watersheds, which contradicts the conventional consideration of autarkic watersheds. The proposed network approach illustrates atmospheric pathways and enables the objective assessment of freshwater vulnerability and water scarcity risks under global change. The illustrated watershed interdependence emphasizes the need for global water governance to secure freshwater availability.

1. Introduction

Today, only 2.5% of the world's water is freshwater available to humans (Oki & Kanae, 2006). Despite living in a *Blue Planet*, annually, more than 4 billion people experience water scarcity worldwide (Mekonnen & Hoekstra, 2016; Vörösmarty et al., 2000). Developing economies in regions with strong seasonal climate variability are the most prone to suffer the consequences of water scarcity (Rijsberman, 2006). However, the rising population and water demand per capita to meet agricultural, industrial, and domestic needs, along with the ongoing depletion of nonrenewable groundwater resources, are posing threats to water security worldwide (e.g., Famiglietti, 2014; Jaramillo & Destouni, 2015; Kummu et al., 2016; Rodell et al., 2018; Wheater, 2015). In some regions, this situation is aggravated by ongoing climate change and the subsequent increase in drought occurrence (Dai, 2013; Sheffield & Wood, 2008) and is expected to continue exacerbating as we progress into the future (e.g., Greve & Seneviratne, 2015; McDonald et al., 2011; Postel, 2000; Schewe et al., 2014; Vörösmarty et al., 2000). This state of affairs has already started to foster competition for water resources between upstream and downstream populations and even between cities and their rural surrounding (Flörke et al., 2018), culminating in several international crises in recent years (e.g., Green et al., 2015; Vörösmarty et al., 2010). Therefore, the United Nations has declared water security as a Sustainable Development Goal (United Nations, 2015), which entails both the protection against hydrometeorological hazards, such as floods and droughts, and the provision of water resources in sufficient quantity and quality to sustain drinking water supply, food production, and ecosystem functioning (Young et al., 2015). Padowski et al. (2015) indicate the importance of the institutions that manage water quantity (and quality) to regulate freshwater availability and mitigate physical and economic water scarcity (Rijsberman, 2006). These management strategies are typically put in practice at the scale of a watershed—that is, the land area characterized by drainage into a common river and a subsequent lake or ocean—and follow the underlying assumption that watersheds are largely independent from their surrounding, self-sustaining and thereby the "best scale at which to govern water" (Cohen, 2012).

Water scarcity is often diagnosed based on the average freshwater availability per capita, using indicators that relate water availability to water demand (e.g., Falkenmark et al., 1989). However, most of these indicators consider only "blue water" availability—that is, rivers, lakes, and groundwater—and thus undermine the importance of soil moisture and return flows from terrestrial evaporation (or evapotranspiration) as local "green water" supplies (Liu et al., 2017). Moreover, water scarcity indicators typically do not consider variability in freshwater supply (Kummu et al., 2010) or changes in atmospheric demand for water, which are

crucial for assessing freshwater availability during droughts (Vicente-Serrano et al., 2010). Only a few studies include green water through consumption (Rockström et al., 2009) or uncertainties related to precipitation (Orth et al., 2016) as a water supply to assess the risk for water scarcity (Veldkamp et al., 2016). Besides these endogenous factors affecting water security, the explicit incorporation of nonlocal, exogenous factors on water supply vulnerability is mostly restricted to virtual water imports, that is, the import of water-intensive products (Dalin et al., 2012; Dalin et al., 2017).

However, blue and green water availability are also subject to the balance between the supply by precipitation and the "loss" by evaporation; and the latter adds moisture to the atmosphere that will eventually precipitate and contribute to freshwater availability. When this precipitation occurs over the same region where water was evaporated, we refer to "precipitation recycling" (Brubaker et al., 1993; Dirmeyer et al., 2009; Eltahir & Bras, 1996; Trenberth, 1999). While the importance of evaporation as a moisture supply for precipitation has received much attention as a land-atmosphere feedback mechanism (e.g., Koster et al., 2004; Miralles et al., 2019; Schär et al., 1999; Seneviratne et al., 2010), it has not received analogous attention in the frame of water resource management and research. However, globally, around 57% of terrestrial evaporation returns as precipitation over land, and 40% of terrestrial precipitation is estimated to be of continental origin (Van der Ent et al., 2010). Especially during dry periods, such as droughts, precipitation shows an increased dependency on terrestrial evaporation (Miralles et al., 2016). Moreover, given multiday residence times of water vapor in the atmosphere and average wind speeds—often much higher than the flow velocity in terrestrial rivers—water vapor can travel long distances once evaporated (e.g., Ramos et al., 2019; Van der Ent & Savenije, 2011). The corresponding climatological source area of moisture for precipitation for a certain region is often referred to as its "precipitationshed," an atmospheric analogue to the terrestrial watershed (Keys et al., 2012; Keys et al., 2018), and may expand way beyond the limits of watersheds. This also implies that human water management and land-use activities affecting evaporation may impact the rainfall in regions far beyond geographical and political boundaries (de Vrese et al., 2016; Gordon et al., 2005; Keune et al., 2018; Keys et al., 2017; Wang-Erlandsson et al., 2018). Moreover, while droughts first affect local blue water availability (Orth & Destouni, 2018), subsequent evaporation deficits influence remote precipitation, which suggests that droughts can self-propagate spatially (Herrera-Estrada et al., 2019; Miralles et al., 2019; Schumacher et al., 2019). Consequently, water resource vulnerability and sustainability are not to be considered solely an issue of local actions but need to be subject to water management and water governance at the global scale (Vörösmarty et al., 2015). This paradigm requires continental- to global-scale and integrated assessments of water resources (Bierkens et al., 2015).

In this study, we provide evidence that supports the need to move away from the more traditional watershed perspective inherited in hydrological sciences, to successfully address global water security challenges. We propose a *watershed precipitation recycling network* to assess the vulnerability of freshwater resources. The network builds upon the concept of watersheds and precipitation recycling through precipitationsheds, establishes atmospheric pathways across watershed boundaries using a Lagrangian trajectory model, and quantifies the independence and interdependence of watershed freshwater resources. In contrast to previous work (e.g., Keys et al., 2017, which focused on country-based exchange of water), we aim to establish a climate network based on the principles of the watershed, including not just its physical characteristics but also the limitations of watershed-based water management. Using European watersheds as an example, we highlight the most and least autarkic watersheds from an atmospheric perspective. Finally, to emphasize the importance of atmospheric connections, we compare estimated volumes of recycled water to thresholds often used to assess physical and economic water scarcity.

2. Methods and Data

In this study, moisture source-sink relationships among European watersheds are identified using the Lagrangian particle dispersion model FLEXPART-ERA-Interim, bias-corrected with daily observations of precipitation. The corresponding source-sink relationships are aggregated to the watershed scale.

2.1. Watersheds

The analysis in this study is based on the geographical delineation of watersheds from the HydroSHEDS data set (Lehner et al., 2006). For simplicity, these are combined into 51 major watersheds as defined by the Food and Agriculture Organization (FAO, 2016; Figure S1 in the supporting information). All major European

watersheds, except for the Arctic Ocean Islands, are used. Watershed populations are calculated using the Gridded Population of the World (v4.10) data set for the year 2015 with a resolution of 15 arc-minutes (Center for International Earth Science Information Network—CIESIN—Columbia University, 2017).

2.2. FLEXPART-ERA-Interim

The Lagrangian particle dispersion model FLEXPART (Stohl et al., 2005) is applied to identify the origin of moisture for precipitation. FLEXPART traces air parcels through the atmosphere and allows to establish source-sink relationships through the evaluation of parcel properties along its trajectory. Despite its original design for dispersion modeling of pollutants, the potential of FLEXPART for tracking atmospheric water vapor has been widely demonstrated (e.g., Drumond et al., 2010; Gimeno et al., 2010; Nieto et al., 2006; Stohl et al., 2008; Stohl & James, 2004; Winschall et al., 2014). Here FLEXPART version 9.01 is driven by ERA-Interim reanalyses at 1° resolution (Dee et al., 2011), and the resulting air parcel trajectories are evaluated. Parcel positions are determined using a Lagrangian motion on top of the transport described by ERA-Interim wind fields. Simulations are performed over extended summers (May–August) from 1980 until 2016, using six-hourly ERA-Interim reanalyses (00, 06, 12, and 18 UTC) and respective three-hourly forecasts (03, 09, 15, and 21 UTC). The use of three-hourly forecasts has been shown to improve the accuracy of the simulated trajectories (Pisso et al., 2010), but only six-hourly outputs, based on the actual reanalysis, are used for the analysis of water budgets. FLEXPART is setup over a continental domain covering Europe and Western Asia (i.e., 60°W–80°E, 20°N–80°N). This nested version uses the global ERA-Interim fields (three-dimensional fields of horizontal and vertical wind, temperature, and specific humidity; and two-dimensional fields of surface pressure, cloud cover, 2-m temperature and dew point temperature, precipitation, sensible and latent heat fluxes, and N/S and W/E surface stress) and a boundary condition, which re-injects a new parcel every time a parcel leaves the domain, preserving a constant number of parcels over time (Stohl et al., 2005).

The described setting allows us to track approximately 2 million parcels over the study domain, which corresponds to an average of approximately 350 parcels per atmospheric column on a $1° \times 1°$ degree grid cell. This nested version and the higher density of parcels per surface compared to previous studies were chosen to improve accuracy, the representation of subgrid-scale processes, and the identification of precipitation and evaporation events. FLEXPART is run in forward mode with 900-s synchronization and sampling time steps. Time steps are, however, adapted to the Lagrangian timescales in order to increase the interaction between horizontal and vertical wind components, which results in a better representation of turbulence (Stohl et al., 2005). The subgrid terrain effect parameterization is employed to increase mixing heights arising from topographic variance at the grid cell level. Analogously to ERA-Interim, the Emanuel (1991) convection scheme is applied. The model output comprises six-hourly binary output files with parcel positions (longitude, latitude, and height) and properties (temperature, density, and specific humidity), and the surrounding boundary layer height for each of the two million parcels; and enables a process-based analysis of individual trajectories.

2.3. Moisture Source Allocation for Precipitation Events

Using FLEXPART, specific humidity changes along a parcel trajectory are interpreted as sources (evaporation) or sinks (precipitation) of moisture, through

$$m\frac{\mathrm{d}q}{\mathrm{d}t} \approx e - p \tag{1}$$

with specific humidity q and moisture increase and decrease rates e and p, respectively. Using ERA-Interim data, the time derivative is approximated using absolute changes of q [kg/kg] over 6-hr time intervals, that is, $\mathrm{d}q/\mathrm{d}t = \Delta q/\Delta t$. Each parcel's mass m [kg] is assumed constant based on the atmospheric mass over the domain and the number of parcels. Over an area A, a large number of parcels, and a sufficient large time period, e and p approximate evaporation E and precipitation P, respectively (Stohl & James, 2004). In order to disentangle signal from noise and to attribute processes in a physically consistent manner—for example, phase changes due to the formation or dissolution of clouds—e and p are defined based on thresholds. Here the process-based moisture source attribution algorithm by Sodemann et al. (2008) is applied and adjusted—as described below—and the resulting fractions are aggregated over watersheds to yield unique source-sink relationships for summer precipitation (June–August). Therefore, first, for all six-hourly time steps for the

evaluation period from 1 June, 00 UTC, until 31 August, 18 UTC, parcels precipitating over a specific watershed are selected, and subsequently, their 10-day backward trajectories are evaluated. To further account for the uncertainty of the established source-sink relationships, analysis is based on a 16-member ensemble using variable thresholds for four parameters used to detect e and p (see the following description and Table S2), which results in different subsets of trajectories for evaluation and subsequent nonlinear variations of the source-sink relationship, while maintaining a reasonably small bias (not shown).

In the following paragraph, we provide a brief description of the moisture source attribution from Sodemann et al. (2008), which defines process-based criteria to detect p and e from individual trajectories and introduces a mass-conserving and physically consistent algorithm to establish source-sink relationships. If not noted otherwise, thresholds from Sodemann et al. (2008) are reported, and their variation for our ensemble is included in brackets. A precipitation event is defined if $q < 0$ g/kg ($q < -0.1$ g/kg), and the mean relative humidity between two time steps exceeds 80% (90%). In order to identify moisture sources for a particular precipitation event, the parcel trajectory is followed backward for 10 days, which corresponds to the mean residence time of water vapor in the atmosphere (Van der Ent & Tuinenburg, 2017) and a commonly assumed limit for trajectory accuracy (e.g., Stohl, 1998). As in Sodemann et al. (2008), the respective backward trajectories are shortened if a parcel dries out ($q < 0.05$ g/kg), and moisture uptakes along the parcel trajectory are (linearly) scaled based on subsequent moisture losses and uptakes. That means that all prior uptakes to a moisture loss are discounted by the fraction of the moisture loss to the specific humidity prior to the moisture loss (i.e., the relative loss; cf. Sodemann et al., 2008, for details). The contribution of an uptake prior to another uptake is similarly discounted (i.e., the scaled uptake is multiplied with the relative contribution of the uptake to the specific humidity prior to the precipitation event analyzed). Moreover, an uptake is considered to be surface evaporation only if the uptake takes place in the vicinity of the boundary layer and exceeds a threshold of 0.2 g/kg (0.3 g/kg) during the 6-hr interval. Here the vicinity of the boundary layer is defined as 1.5 (1.25) times the mean boundary layer height of two consecutive time steps. Note that this differs from the original proposition by Sodemann et al. (2008), in which only oceanic boundary layer heights were multiplied with a relaxation factor. We adopted this criterion for all uptakes in order to account for the diurnal cycle of terrestrial boundary layer heights. Uptakes that occur prior to the 10-day backward trajectory or that do not meet these requirements are considered as undefined sources or noise. The mathematical formulations for this moisture source allocation algorithm can be found in Sodemann et al. (2008). This algorithm allows us to determine the sources of moisture for precipitation in a realistic and mass-conserving manner, as it provides fractional weights f_w of the contribution of each defined evaporation event to each defined precipitation event. More specifically, regarding a single parcel trajectory, for which n uptakes and uptake locations are defined to contribute to a moisture loss q_p at a specific time and place, we define

$$\Delta q_P = \sum_i^n f_{w,i} \cdot \Delta q_P + \left(1 - \sum_i^n f_{w,i}\right) \cdot \Delta q_P \tag{2}$$

where

$$F = \sum_i^n f_{w,i} \tag{3}$$

is the fraction of explained moisture uptakes. The remainder, that is, $(1 - F)$, is the fraction of precipitation that cannot be explained by surface evaporation using FLEXPART. This is due to the criteria that define uptakes as surface evaporation (i.e., within the vicinity of the boundary layer and above a certain threshold), as well as the application of a nested domain and the assumption of a maximum residence time for water vapor in the air, which limit the trajectory length. The determination of f_w and the number of uptakes that leads to F is analogous to the algorithm proposed by Sodemann et al. (2008) and bias-corrected on a daily basis.

Finally, precipitation and evaporation events are defined at the median position of two consecutive time steps and are accordingly attributed to the watersheds used in this study. The aggregation of f_w over millions of parcels over time and space allows us to determine unique source-sink relationships between watersheds. More specifically, we determine the fraction of precipitation in watershed X that is

associated with surface evaporation in watershed Y, for all unique combinations of X and Y. The sum over time over all uptakes n in watershed Y for each precipitating parcel p in watershed X then yields the unique source-sink weight

$$F(X,Y) = \frac{\sum_{p}^{P}\sum_{i}^{n} f_{w,i}\cdot\Delta q_P\cdot 1_{f,Y}}{\sum_{p}^{P}\Delta q_P\cdot 1_X} \tag{4}$$

where 1_X ($1_{f,Y}$) is a function that returns one if precipitation (evaporation) is allocated to watershed X (Y) and collapses to zero otherwise. The definition of fractional weights as contributions to precipitation allows us to directly apply the identified source-sink relationships to observed watershed precipitation (see section 2.4), that is,

$$E_Y = F(X,Y)\cdot P_{X,\mathrm{obs}} \tag{5}$$

which indicates that 100 × $F(X,Y)$% of precipitation P in watershed X is recycled from evaporation E in watershed Y. The combination of the FLEXPART-determined source-sink relationships with an observational precipitation product allows us to circumvent the impact of potential biases in the precipitation estimates from FLEXPART. It is, however, noted that the accuracy of the moisture source allocation algorithm is affected by a series of assumptions, such as the ones explained above. Moreover, condensation and vaporization due to the formation or dissolution of clouds are neglected, and the associated specific humidity changes can be misinterpreted as terrestrial evaporation or precipitation events (Stohl & James, 2004). Other phase changes, such as sublimation and deposition, are not explicitly accounted for either but are expected to represent nonsignificant contributions (Stohl & James, 2004). The same holds for parcels that entrain or escape the (vicinity of the) planetary boundary layer: a precipitating parcel that escapes the boundary layer cannot be accounted for; likewise, a parcel that enters the boundary layer and gains moisture might be misinterpreted as evaporation (Stohl & James, 2004). Last but not least, the relatively large time step of 6 hr, during which evaporation and precipitation can occur simultaneously, increases the uncertainty in the definition of source and sink amount and location. To account for this uncertainty associated with the definition of precipitation and evaporation events, the above-described 16-member ensemble is performed. Reported results are based on the ensemble mean and range.

2.4. Precipitation Recycling and External Land Source Contributions

The sources of moisture for precipitation in watershed X are attributed to (i) the watershed itself, (ii) any other European watershed considered in this study ($Y \neq X$), or (iii) other undefined source regions, that is, land outside Europe or water bodies, such as ocean and lakes. Based on this division, the total, observed precipitation amount can be subdivided into these three categories, that is,

$$P_{X,\mathrm{obs}} = F(X,X)\cdot P_{X,\mathrm{obs}} + \sum_{Y\neq X} F(X,Y)\cdot P_{X,\mathrm{obs}} + \left(1-\sum_{Y} F(X,Y)\right)\cdot P_{X,\mathrm{obs}} \tag{6}$$

with the latter term accounting for undefined sources not identifiable with FLEXPART as well as extra-European land and oceanic sources (hereafter referred to as extra-Europe). We define a watershed Precipitation Recycling Ratio (*PRR*) as follows:

$$PRR = \frac{F(X,X)\cdot P_{X,\mathrm{obs}}}{P_{X,\mathrm{obs}}} \tag{7}$$

and an External Land-origin Precipitation Ratio (*ELPR*) that defines the contribution from other European watersheds to X as follows:

$$ELPR = \frac{\sum_{Y \neq X} F(X,Y) \cdot P_{X,\text{obs}}}{P_{X,\text{obs}}} \quad (8)$$

Therefore, the former describes the self-reliance of the watershed X to produce its own precipitation, and the latter describes the dependence of the watershed X on other (European) watersheds. The contribution of terrestrial Europe to precipitation in watershed X results from the sum of these two contributions:

$$LPR = PRR + ELPR, \quad (9)$$

and illustrates the Land-origin Precipitation ratio (*LPR*). The remainder ($1 - LPR$) is the fraction of precipitation in watershed X that originates from the ocean, non-European land regions, or cannot be explained with FLEXPART, and accounts for preexisting moisture contents of air parcels. It is noted here that these recycling ratios may represent upper estimates of land contributions, as the moisture source attribution algorithm proposed by Sodemann et al. (2008) in combination with FLEXPART-ERA-Interim yields residence times of water vapor in the atmosphere that are in the low end of reported values (Van der Ent & Tuinenburg, 2017) and may hence overestimate the contribution of nearby source regions. To mitigate this effect, source-sink relationships are calculated and corrected with observations of precipitation on a daily basis.

2.5. Observations

Observed precipitation is taken from the Multi-Source Weighted Ensemble Precipitation product (MSWEP v.1.2, Beck et al., 2017), which is a synthesis of gauge measurements, reanalysis, and satellite observations. Analogously, to compare volumes of evaporation leading to precipitation, the observation-driven evaporation product from the Global Land Evaporation Amsterdam Model (GLEAM v.3.2, Martens et al., 2017; Miralles et al., 2011) is used. GLEAM constrains potential evaporation estimates using a water stress function based on observations of precipitation, soil moisture, and vegetation optical depth. Here watershed averages of MSWEP precipitation and GLEAM evaporation are calculated based on the fractional spatial overlap of watershed and grid cell area (Figure S4). This overlap of a grid cell with the watershed is calculated based on a subdivision of each grid cell into 100 subgrid cells. The resulting grid cell weights are then multiplied with grid point observations and averaged per watershed. This procedure replaces a normalization with the watershed area. Climatological watershed-averaged precipitation and evaporation from MSWEP and GLEAM are shown in Figure S5.

3. Results and Discussion

3.1. Watershed Independence

Part of the precipitation in any given watershed will originate from atmospheric moisture generated through evaporation within the watershed itself. This "self-supply of water" is illustrated in Figure 1a as a ratio (see *PRR* in equation (7)). Mean values range from ~0.02 (Scheldt; ensemble range from 0.015 to 0.019) to ~0.30 (Danube; ensemble range from 0.28 to 0.32), which means that the Scheldt only supplies ~2% of moisture for its own summer precipitation, while the Danube is much more self-reliant (or independent), as ~30% of its summer precipitation supply originates from local evaporation. There is an obvious dependency of these ratios on the watershed size as the recycling ratio of moisture increases with area (Dirmeyer & Brubaker, 2007; Van der Ent & Savenije, 2011); as such, large watersheds are expected to be more self-reliant than smaller watersheds. Here larger recycling ratios are evident for larger watersheds, such as the Danube or Volga, which encompass 799,650 and 1,474,073 km^2, respectively (Figure 1a). Nonetheless, these results show that watersheds are far from being autarkic systems but strongly depend on moisture supply from other watersheds and the ocean and seas. Figure 1b shows, for each watershed, the fraction of summer precipitation that is supplied by evaporation from other European watersheds (*ELPR*) and thus illustrates the degree of interdependence. These values exceed the self-supply for all watersheds in continental Europe and range from ~0.09 (Iceland; ensemble range from 0.086 to 0.093) to ~0.74 (Daugava; ensemble range from 0.73 to 0.76). Adding the two ratios (*PRR* and *ELPR*), we find an increasing gradient in the contribution of precipitation originating from European territories (*LPR*) from Western to Eastern Europe (Figures 1 and S7). This gradient results from the predominant westerly winds and the decreasing influence of the Atlantic Ocean from

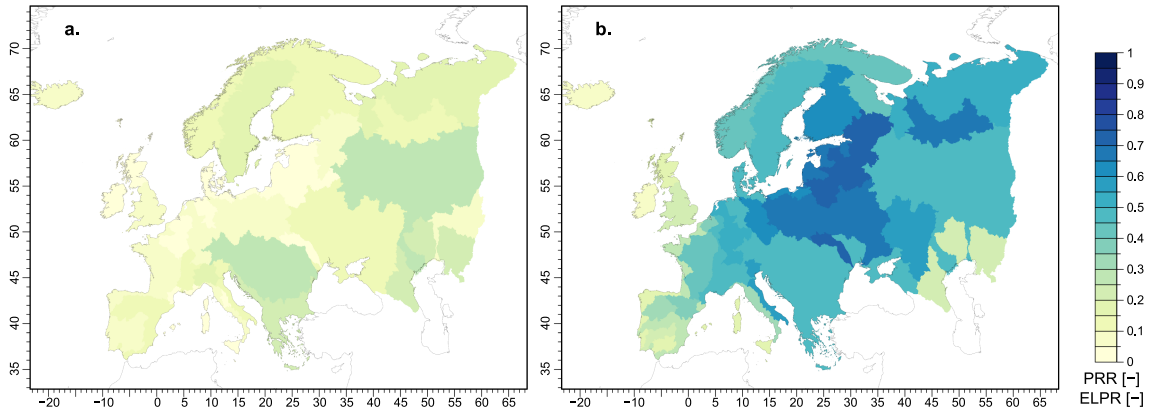

Figure 1. Sources of moisture for summer precipitation over the 50 major European watersheds for the years 1980–2016: (a) fraction of precipitation supplied by the watershed itself ("self-supply," *PRR*) and (b) fraction of precipitation supplied by other European watersheds ("supply by other watersheds," *ELPR*). Values represent the ensemble mean.

Western Europe to Eastern Europe (Gimeno et al., 2012; see Figure S11). During European summers, watersheds in Iceland receive approximately 88% (ensemble range: 87–88%) of moisture for precipitation from outside Europe including the ocean and only ~9% (ensemble range: 8.6–8.8%) from other European watersheds. On the contrary, inland watersheds are much more dependent on evaporation from other watersheds. The Northern Dvina receives only ~19% (ensemble range: 19.1–19.5%) of its precipitation from the ocean. The resulting *LPR* values are comparable to those found by Van der Ent et al. (2010) and Brubaker et al. (1993) but are higher than the ratios reported by Bisselink and Dolman (2009), Dirmeyer and Brubaker (2007), and Berger et al. (2018), which may result from the differences in methodological tools and their assumptions. Nonetheless, these ratios are highly dependent on the underlying area and time period being considered when computing precipitation recycling.

3.2. The Watershed Precipitation Recycling Network

The dependency of a watershed on moisture supply for precipitation from other watersheds, as illustrated in Figure 1b, can be decomposed into the contributions from individual watersheds. If this decomposition is repeated for all watersheds, a "watershed precipitation recycling network" can be constructed, such as the one illustrated in Figure 2 in the form of a chord diagram. European watersheds are arranged according to six geographical regions (see Figure S2): Western (orange), Mid- (purple), Northern (green), Eastern (blue), Southeastern (yellow), and Southern Europe (red). In addition, extra-European source regions (ocean and other land areas) are illustrated in black, but the precipitation in those regions is not shown (see Figure S8 for a chord diagram also excluding extra-European sources). Bars in the inner circle of the chord diagram represent individual watersheds, and their arc width is proportional to the contributed and received volumes of water (km^3), that is, their evaporation supply and precipitation dependency within the network. The lines show the flow of atmospheric moisture from the source watershed (indicated by a small gap between the watershed bar and the flow line) to the sink watershed (indicated by arrows toward the bar representing the watershed) and are colored by the geographical location of the source watershed. Inspection of precipitation in one watershed hence enables the direct identification of the corresponding source watersheds.

The chord diagram illustrates that watersheds in Eastern, Northern, and Mid-Europe play a key role in the summertime precipitation recycling network over Europe. Watersheds in Western, Southern, and Southeastern Europe supply moisture to watersheds across Europe but receive most of the moisture for precipitation from the ocean. Inspecting single watersheds, the Volga and the Danube emerge as pivotal, presumably because of their size and central location. They portray, however, also the most effective contributions when volumes are normalized by area (see Figures S9 and S10). Moreover, even large watersheds show a dependency on moisture supply from other watersheds. Overall, external contributions are mostly arising from watersheds in the same geographical region (nearby watersheds, as indicated by the prevailing colors of each region), but cross-region supply can be paramount. A prominent example is the supply of moisture from Mid-Europe to Eastern and Southeastern Europe and, for example, the supply of moisture for precipitation from the Danube to the Dnieper and watersheds at the Adriatic and Black Sea coast.

Figure 2. Climatological chord diagram visualizing the watershed precipitation recycling network for the 50 major European watersheds during summertime (1980–2016). Lines between watersheds illustrate the quantitative source-sink relationships between evaporation [km^3/summer] and precipitation [km^3/summer], based on the ensemble mean. Colors represent the region of the source watershed. Flows are illustrated from the evaporating watershed (represented by a gap between the watershed bar and flow line) to the precipitating watershed (represented by an arrow toward the watershed bar). For better illustration, contributions below the 0.1 quantile of all contributions are not represented.

Inspection of the watershed precipitation recycling network in Figure 2 furthermore enables the identification of network structures, that is, moisture pathways, similar to the atmospheric connections recently identified among countries by Keys et al. (2017). One example of these pathways and their cascading effects is illustrated here: a large percentage of summer precipitation over the Loire originates from extra-European regions; this precipitation is partly returned to the atmosphere through evaporation and supplies moisture for precipitation over the Rhine, which in turn contributes to the precipitation over the Danube, which supplies moisture to the Dnieper, and so on. The existence of such network structures enables spatial drought propagation (Miralles et al., 2019; Zemp et al., 2017), which highlights the need to develop integrated land and water resource management strategies to approach continental to global water governance.

For better inspection and explanation of individual interwatershed connections, Figure 3 illustrates watersheds acting as climatological sources and sinks of moisture for and from the Volga, Danube, and Loire. Figure 3a illustrates the watersheds supplying precipitation to the Volga, that is, the source watersheds, analogous to the concept of precipitationsheds (Keys et al., 2014). Approximately 28% of summer precipitation over the Volga originates from the Volga watershed itself (84.53 km^3), ~23% originates from the ocean and extra-European land (69 km^3), followed by large contributions from the Don (~7%;19.66 km^3), Dnieper

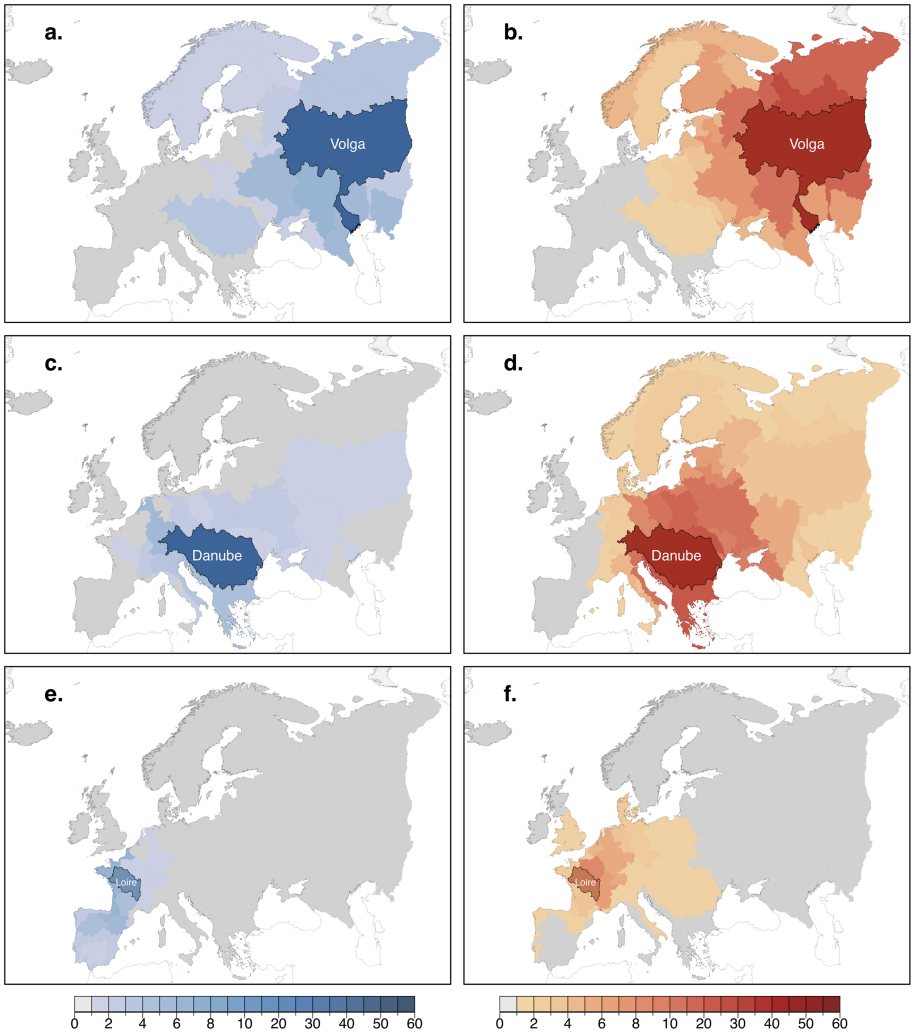

Figure 3. Watersheds supplying (blue) and receiving (orange) moisture for precipitation to and from (a, b) the Volga, (c, d) Danube, and (e, f) Loire. Colors indicate the ensemble mean *PRR* [%] and *ELPR* [%] contributions from and to the source and sink watersheds, respectively. Contributions below 1% are masked in grey. Results correspond to summertime (1980–2016).

(~6%; 17.63 km^3), watersheds at the Caspian Sea Coast (~6%; 16.96 km^3), and the Northern Dvina (~4%; 11.05 km^3). Analogously, Figure 3b illustrates the watersheds in which moisture evaporated from the Volga precipitates, that is, the sink watersheds. Among others, evaporation from the Volga watershed contributes to precipitation over the Northern Dvina (~26% of its precipitation; 14.66 km^3), Ural (~17%; 3.68 km^3), watersheds at the Russian Barents Sea Coast (~16%; 21.67 km^3), Neva (~13%; 5.95 km^3), and Don (~12%; 8.00 km^3).

Figures 3c–3f illustrate the equivalent sources and sinks for the Danube and Loire. Watershed connections for the Danube are similar to those described for the Volga, with the largest contributions coming from the Danube itself (~30% 55.98 km^3), followed by extra-European sources (~20%; 39.22 km^3), the Rhine (~5%; 9.67 km^3), and watersheds at the Adriatic Sea Coast (~5%; 8.69 km^3). The Dniester shows a strong dependency on moisture supply from the Danube (~25%; 3.08 km^3) and so do the watersheds on the Adriatic Sea Coast (~21%; 6.25 km^3), Wisla (~17%; 6.30 km^3), Dnieper (~14%; 13.66 km^3), and watersheds on the East Coast of Italy (~13%; 1.79 km^3). Due to the predominant westerly winds (see Figure S11), the source watersheds for precipitation over the Loire are located over the Iberian Peninsula, France, and the United Kingdom, while sink watersheds are shifted toward the East, from eastern France to Mid- and

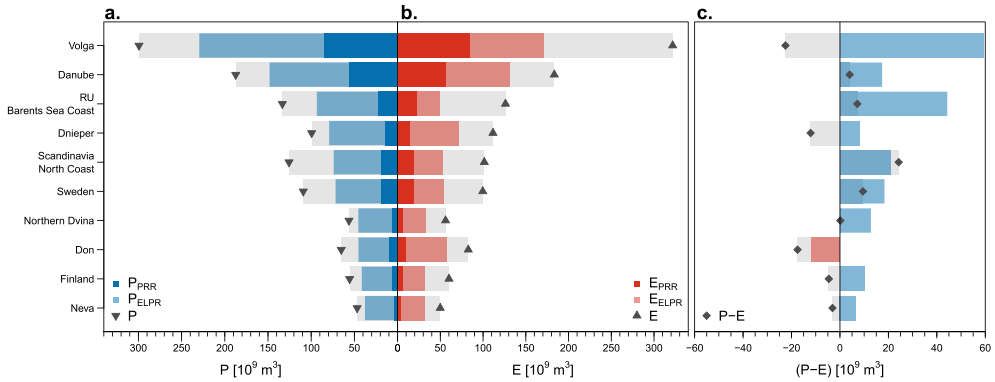

Figure 4. The 10 key watersheds in the watershed precipitation recycling network, ranked according to the average summer precipitation [km^3] received from other watersheds. Observations of (a) precipitation, (b) evaporation, and (c) net freshwater availability ($E - P < 0$) are subdivided into their origin and destination: dark blue (red) colors indicate the total water received (supplied) through terrestrial precipitation recycling from the watershed itself (*PRR*), and light blue (red) colors indicate the total water received (supplied) from other European watersheds (*ELPR*). Grey bars and symbols indicate the total evaporation (GLEAM), precipitation (MSWEP), and their difference ($P - E$), respectively. Values represent the ensemble mean.

Eastern Europe (see Figures 3e and 3f). Despite the fact that precipitation over the Loire is largely of extra-European origin (~51%; 8.55 km^3) or comes from local recycling (~8%; 1.28 km^3), a fraction is also supplied by evaporation from watersheds at the west coast of France (~6; 1.07 km^3), Ebro (~5%; 0.90 km^3), Gironde (~5%; 0.80 m^3), and Douro (~5%; 0.78 km^3)—see Figure 3e. Likewise, the Loire supplies moisture for precipitation to the Seine (~8%; 0.91 km^3), Rhone (~7%; 1.24 km^3), Rhine (~5%; 2.20 km^3), Maas (~5%; 0.25 km^3), and Scheldt (~4%; 0.16 km^3)—see Figure 3f. This way of visualizing results helps to understand the role played by each watershed within the precipitation recycling network. Given the predominance of westerly winds, cascading effects within Europe are especially visible for the Loire, with sources from the Iberian Peninsula and sinks across central Europe. As expected, for example, due to prevailing winds, the source-sink exchange between any two watersheds is usually not balanced out.

3.3. Key Actors in the European Watershed Precipitation Recycling Network

As illustrated before, substantial fractions of summer precipitation in Europe are supplied by terrestrial evaporation within Europe; thus, the corresponding exchange of water among watersheds comprises large volumes. This interwatershed exchange is illustrated in Figure 4 for the 10 watersheds that receive the largest volumes of precipitation from other watersheds, with the three largest volumes arriving in the Volga, Danube, and at the Russian Barents Sea Coast (see light blue bars in Figure 4a). These are also the top suppliers of precipitation to other watersheds (see pale red bars in Figure 4b), which makes them key actors in the precipitation recycling network (see also Figure 2). There are, however, imbalances within the precipitation recycling network: most of these key watersheds receive more moisture from other watersheds than they supply back to them (see light blue bars in Figure 4c). This within-network imbalance can, however, diverge from the total net freshwater availability ($P - E$), which is also affected by extra-European sources and sinks (see grey bars in Figure 4c). The Danube, for example, receives more moisture from other watersheds than it supplies to them (see light blue bar in Figure 4c), which contributes to a net terrestrial freshwater availability ($P - E > 0$; see grey bar in Figure 4c). The same holds for watersheds at the Russian Barents Sea Coast, Sweden, and Scandinavian North Coast.

Simultaneously, some watersheds, such as the Don, experience a net loss of water from the land surface during summer (see grey bars in Figure 4c, where $(P - E) < 0$). This is partly caused by their supply of precipitation to other watersheds exceeding the precipitation they receive from them (see pale red bar in Figure 4c). Beyond that, a watershed can receive more precipitation from other watersheds than it supplies but simultaneously experience a total net loss of freshwater (see divergence between light blue and grey bars for Volga, Dnieper, Finland, and Neva in Figure 4c). These differences between observed and recycled volumes emerge due to the contributions from (to) extra-European sources (sinks), for example, the Volga receives more moisture from European watersheds than it supplies to them (see light blue bar in Figure 4c), but it

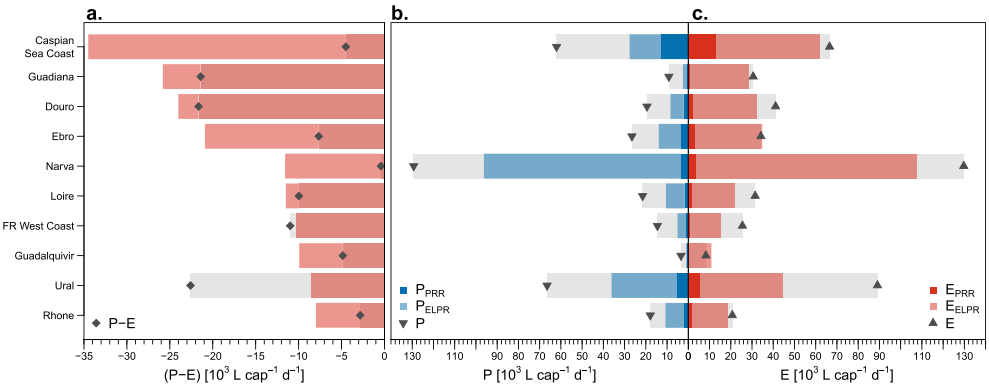

Figure 5. Top 10 watersheds experiencing a net loss of freshwater in liters per capita per day during summer due to precipitation recycling within Europe. Observation-driven estimates of (a) the net freshwater loss ($P < 0$), (b) precipitation, and (c) evaporation are subdivided into their origin and destination: dark blue (red) colors indicate the total water received (supplied) through terrestrial precipitation recycling within the watershed itself (*PRR*), light blue (red) colors indicate the total water received (supplied) from (to) other European watersheds (*ELPR*). Grey bars and symbols indicate the total evaporation (GLEAM), precipitation (MSWEP), and their difference ($P - E$), respectively, and thus include extra-European sinks and sources.

supplies more moisture for precipitation to Extra-European regions not considered in this study, hence resulting in a total ($P - E$) < 0 (see grey bar in Figure 4c). This consideration of evaporation as a contributor to precipitation highlights the vulnerability of freshwater resources, as water deficits ($P - E <$ 0) may reflect a natural supply to other watersheds which needs to be locally compensated through other sources of water.

3.4. Implications for Water Scarcity and Freshwater Vulnerability

The importance of considering the origin of freshwater is evidenced when the volumes of recycled water are evaluated in the context of water scarcity and water resource vulnerability. Here we illustrate the "natural trade of freshwater" by evaluating people's natural dependency on water supply during summer (*How much freshwater does a person on average receive from other watersheds?*), their own supply to people in other watersheds (*How much freshwater does a person on average "supply" to people in other watersheds?*), and the imbalance between those two. Of key interest are watersheds in which the supply overcomes the received volumes, as their net imbalance can be a sign of vulnerability to water scarcity. For these more vulnerable watersheds, Figure 5a illustrates the net loss of freshwater per capita during summer; again this net loss results from the natural trade of freshwater among watersheds through the atmosphere. Watersheds in Figure 5 are ranked according to the magnitude of their imbalance, that is, the difference between the average per capita volumes of supplied/received water to/from all other watersheds. While light red bars in Figure 5c illustrate the natural supply of water per person to precipitation in other watersheds, the light blue bars in Figure 5b illustrate the corresponding volumes per person that are received from other watersheds; the difference between these two yields the light red bars in Figure 5a, that is, the net loss of freshwater per capita. This imbalance illustrates the amount of water that needs to be compensated by other water sources, such as reservoirs and groundwater.

With a net water availability ($P - E$) of less than −32,000 L per capita per day, the average person living at the Caspian Sea Coast "supplies" much more water to other watersheds during an average summer than it receives from them (see light red bar in Figure 5a). The Narva watershed receives around 90,000 L of freshwater per capita per day from its surrounding watersheds (see light blue bar in Figure 5b); however, more than 100,000 L per capita per day are supplied for precipitation in other European watersheds (see light red bars in Figure 5c), leading to a net deficit of about 10,000 L (see light red bar in Figure 5a). The volumes of precipitation coming from outside Europe balance this deficit ($P - E \approx 0$; see grey point in Figure 5a). Notably, also watersheds in the Iberian Peninsula—namely Guadiana, Douro, Ebro, and Guadalquivir—and at the West Coast of France, supply more water via evaporation to other European watersheds than they receive via precipitation from them (see pale red bars in Figure 5a); therefore, these Iberian watersheds also

experience a net loss of freshwater during summer, which unlike for the Narva, is not balanced by extra-European inputs and leads to a deficit ($P - E < 0$; see grey bars in Figure 5a).

It is important to note that values in Figure 5a only illustrate the natural deficit of freshwater, arising from recycled precipitation and evaporation. Nonetheless, the net deficit resulting from interwatershed transfers (pale red bars) already exceeds on its own annual water scarcity thresholds (1,500 $m^3 \cdot cap^{-1} \cdot year^{-1}$ = 4,100 $L \cdot cap^{-1} \cdot day^{-1}$; Falkenmark et al., 1989) in all watersheds. These volumes even exceed the average European water footprint including the trade of virtual water (~5,000 L $cap^{-1} \cdot day^{-1}$; Vanham & Bidoglio, 2013). While our estimates only refer to summer months, during which deficits are expected to be largest, they suggest a dominant role of the natural water cycle for freshwater deficits, which propagate through the atmospheric precipitation recycling network and further affect remote water resources. More importantly, the need to compensate these natural deficits via water management, including freshwater withdrawals (e.g., ~2,000 $L \cdot cap^{-1} \cdot day^{-1}$ in Italy), increases the pressure on water resources (e.g., groundwater and surface reservoirs) and subsequently raises the risks of water scarcity. For comparison, food trade has been shown to contribute to groundwater depletion, with volumes ranging from ~32 to 167 $L \cdot cap^{-1} \cdot day^{-1}$ embedded in food trade from Italy to Germany and from Bulgaria to Romania, respectively (Dalin et al., 2017). Hence, the natural "atmospheric trade" of water between watersheds exceeds the footprint of water embedded in food trade. This suggests that the propagation of freshwater deficits in space, as illustrated by the network dependencies, may serve as a main driver of groundwater depletion during summer.

4. Summary and Conclusion

Despite conventional assumptions based on a terrestrial perspective of hydrology, our findings illustrate that watersheds are far from being autarkic systems, as they are highly dependent on moisture supplied by other watersheds through the atmosphere. Using a Lagrangian particle dispersion model, we proved that high percentages of summer precipitation in European watersheds originate from either the watershed itself (precipitation recycling) or from neighbor or remote watersheds. Depending on the watershed, between 9% and 74% of summer precipitation originates from other watersheds. This percentage increases from Western to Eastern European watersheds and decreases with watershed size.

To enhance the process-based understanding of source-sink relationships between watersheds, we proposed the concept of a watershed precipitation recycling network, which visualizes the interdependence of watersheds through atmospheric pathways. Large watersheds, such as Volga and Danube, are found to be much more independent, while simultaneously supplying the largest volumes of precipitation to other watersheds. Nevertheless, even such large watersheds remain somehow dependent on the moisture supplied by other watersheds. During summer, an imbalance in this atmospheric exchange of water between watersheds may lead to natural water deficits. These deficits are shown to exceed local water consumption, freshwater withdrawal, and water scarcity thresholds in some watersheds, particularly in the Mediterranean region. Therefore, natural imbalances in this "atmospheric trade" of water may increase the pressure on local water resources and ultimately contribute to groundwater depletion.

These findings highlight the importance of considering terrestrial evaporation as a supply for precipitation and freshwater availability. Therefore, repercussions of upwind evaporation as a contributor to precipitation downwind should be considered in assessments of freshwater vulnerability. Our results suggest that evaporation anomalies induced by local actions—such as irrigation or land use—may propagate downwind and affect freshwater availability and consequently water management in other watersheds. Following the same logic, droughts and water scarcity may also propagate from watershed to watershed due to the reduced evaporation associated with these events, especially in dry climates. This puts emphasis on the fact that freshwater availability and water use sustainability are global issues that know no political or geographical boundaries (Vörösmarty et al., 2015). They strongly depend on large-scale circulation and land-atmosphere feedbacks, and consequently on land and water management across boundaries. The holistic perspective of a watershed precipitation recycling network may help to better understand the drivers of and threats to water availability and security across the Earth System. The framework allows to address water security challenges at large scales, yet providing guidance to local-scale management. It can be used to analyze remote impacts

arising from local land and water management but also the impacts of localized adaptation strategies on regional to global climate. Ultimately, considering a broader picture that trespasses the limit of watersheds may help to improve early warnings of water scarcity and foster the development of adaptation and sustainability strategies.

Data availability

MSWEP data were downloaded from http://www.gloh2o.org/. GLEAM data are freely accessible via https://www.gleam.eu/. ERA-Interim data are available via https://apps.ecmwf.int/datasets/. Watershed delineations and major basin classification were downloaded from http://www.fao.org/geonetwork/srv/en/main.home?uuid=1849e279-67bd-4e6f-a789-9918925a11a1. Population data from GPW were downloaded from http://sedac.ciesin.columbia.edu/data/set/gpw-v4-population-count-rev10. Chord diagrams were created using the "circlize" library from Zugang Gu (Gu et al., 2014; https://github.com/jokergoo/circlize). Data are available at https://dx.doi.org/10.6084/m9.figshare.9725084 (Keune & Miralles, 2019).

Acknowledgments
The authors acknowledge the support from the European Research Council (ERC) under grant agreement 715254 (DRY-2-DRY). The computational resources and services used in this work were provided by the VSC (Flemish Supercomputer Center), funded by the Research Foundation-Flanders (FWO) and the Flemish Government—department EWI. We thank Stephan Henne, Raquel Nieto, Luis Gimeno, and Anita Drumond for constructive discussions regarding the setup of FLEXPART and the postprocessing of the output. We are furthermore grateful to Dominik Schumacher and Hendrik Wouters for insightful discussions and technical support. The constructive criticisms of the Editor Martyn Clark, the Associate Editor Thorsten Wagener, and the three reviewers (Ruud van der Ent, René Orth, and Jianhui Wei) have been greatly beneficial for the quality of the manuscript.

References

Beck, H. E., Van Dijk, A. I., Levizzani, V., Schellekens, J., Miralles, D. G., Martens, B., & de Roo, A. (2017). MSWEP: 3-hourly 0.25 global gridded precipitation (1979–2015) by merging gauge, satellite, and reanalysis data. *Hydrology and Earth System Sciences*, *21*(1), 589–615. https://doi.org/10.5194/hess-21-589-2017

Berger, M., Eisner, S., van der Ent, R., Flörke, M., Link, A., Poligkeit, J., et al. (2018). Enhancing the water accounting and vulnerability evaluation model: WAVE+. *Environmental Science and Technology*, *52*(18), 10,757–10,766. https://doi.org/10.1021/acs.est.7b05164

Bierkens, M. F. P., Bell, V. A., Burek, P., Chaney, N., Condon, L. E., David, C. H., et al. (2015). Hyper-resolution global hydrological modelling: What is next? "Everywhere and locally relevant". *Hydrological Processes*, *29*(2), 310–320. https://doi.org/10.1002/hyp.10391

Bisselink, B., & Dolman, A. J. (2009). Recycling of moisture in Europe: Contribution of evaporation to variability in very wet and dry years. *Hydrology and Earth System Sciences*, *13*(9), 1685–1697. https://doi.org/10.5194/hess-13-1685-2009

Brubaker, K. L., Entekhabi, D., & Eagleson, P. S. (1993). Estimation of continental precipitation recycling. *Journal of Climate*, *6*(6), 1077–1089. https://doi.org/10.1175/1520-0442(1993)006<1077:EOCPR>2.0.CO;2

Center for International Earth Science Information Network—CIESIN—Columbia University (2017). Gridded population of the world, version 4 (GPWv4): Population count, Revision 10. Palisades, NY: NASA Socioeconomic Data and Applications Center (SEDAC). https://doi.org/10.7927/H4PG1PPM. Accessed 1 March 2019.

Cohen, A. (2012). Rescaling environmental governance: Watersheds as boundary objects at the intersection of science, neoliberalism, and participation. *Environment and Planning A*, *44*(9), 2207–2224. https://doi.org/10.1068/a44265

Dai, A. (2013). Increasing drought under global warming in observations and models. *Nature Climate Change*, *3*(1), 52. https://doi.org/10.1038/nclimate1633

Dalin, C., Konar, M., Hanasaki, N., Rinaldo, A., & Rodriguez-Iturbe, I. (2012). Evolution of the global virtual water trade network. *Proceedings of the National Academy of Sciences*, *109*(16), 5989–5994. https://doi.org/10.1073/pnas.1203176109

Dalin, C., Wada, Y., Kastner, T., & Puma, M. J. (2017). Groundwater depletion embedded in international food trade. *Nature*, *543*(7647), 700–704. https://doi.org/10.1038/nature21403s

de Vrese, P., Hagemann, S., & Claussen, M. (2016). Asian irrigation, African rain: Remote impacts of irrigation. *Geophysical Research Letters*, *43*, 3737–3745. https://doi.org/10.1002/2016GL068146

Dee, D. P., Uppala, S. M., Simmons, A. J., Berrisford, P., Poli, P., Kobayashi, S., et al. (2011). The ERA-Interim reanalysis: Configuration and performance of the data assimilation system. *Quarterly Journal of the Royal Meteorological Society*, *137*(656), 553–597. https://doi.org/10.1002/qj.828

Dirmeyer, P. A., & Brubaker, K. L. (2007). Characterization of the global hydrologic cycle from a back-trajectory analysis of atmospheric water vapor. *Journal of Hydrometeorology*, *8*(1), 20–37. https://doi.org/10.1175/JHM557.1

Dirmeyer, P. A., Schlosser, C. A., & Brubaker, K. L. (2009). Precipitation, recycling, and land memory: An integrated analysis. *Journal of Hydrometeorology*, *10*(1), 278–288. https://doi.org/10.1175/2008JHM1016.1

Drumond, A., Nieto, R., Trigo, R., Ambrizzi, T., Souza, E., & Gimeno, L. (2010). A Lagrangian identification of the main sources of moisture affecting northeastern Brazil during its pre-rainy and rainy seasons. *PLoS ONE*, *5*(6), e11205. https://doi.org/10.1371/journal.pone.0011205

Eltahir, E. A., & Bras, R. L. (1996). Precipitation recycling. *Reviews of Geophysics*, *34*(3), 367–378. https://doi.org/10.1029/96RG01927

Emanuel, K. A. (1991). A scheme for representing cumulus convection in large-scale models. *Journal of the Atmospheric Sciences*, *48*(21), 2313–2329. https://doi.org/10.1175/1520-0469(1991)048<2313:ASFRCC>2.0.CO;2

Falkenmark, M., Lundqvist, J., & Widstrand, C. (1989). Macro-scale water scarcity requires micro-scale approaches: Aspects of vulnerability in semi-arid development. *Natural Resources Forum*, *13*(4), 258–267. https://dx.doi.org/10.1111/j.1477-8947.1989.tb00348.x

Famiglietti, J. S. (2014). The global groundwater crisis. *Nature Climate Change*, *4*(11), 945. https://doi.org/10.1038/nclimate2425

FAO (2016). AQUASTAT main database. Food and Agriculture Organization of the United Nations (FAO). Website accessed on [01/03/2019 7:49].

Flörke, M., Schneider, C., & McDonald, R. I. (2018). Water competition between cities and agriculture driven by climate change and urban growth. *Nature Sustainability*, *1*(1), 51–58. https://doi.org/10.1038/s41893-017-0006-8

Gimeno, L., Drumond, A., Nieto, R., Trigo, R. M., & Stohl, A. (2010). On the origin of continental precipitation. *Geophysical Research Letters*, *37*, L13804. https://doi.org/10.1029/2010GL043712

Gimeno, L., Stohl, A., Trigo, R. M., Dominguez, F., Yoshimura, K., Yu, L., et al. (2012). Oceanic and terrestrial sources of continental precipitation. *Reviews of Geophysics*, *50*, RG4003. https://doi.org/10.1029/2012RG000389

Gordon, L. J., Steffen, W., Jönsson, B. F., Folke, C., Falkenmark, M., & Johannessen, Å. (2005). Human modification of global water vapor flows from the land surface. *Proceedings of the National Academy of Sciences*, *102*(21), 7612–7617. https://doi.org/10.1073/pnas.0500208102

Green, P. A., Vörösmarty, C. J., Harrison, I., Farrell, T., Sáenz, L., & Fekete, B. M. (2015). Freshwater ecosystem services supporting humans: Pivoting from water crisis to water solutions. *Global Environmental Change*, *34*, 108–118. https://dx.doi.org/10.1016/j.gloenvcha.2015.06.007

Greve, P., & Seneviratne, S. I. (2015). Assessment of future changes in water availability and aridity. *Geophysical Research Letters*, *42*, 5493–5499. https://doi.org/10.1002/2015GL064127

Gu, Z., Gu, L., Eils, R., Schlesner, M., & Brors, B. (2014). Circlize implements and enhances circular visualization in R. *Bioinformatics*, *30*(19), 2811–2812. https://doi.org/10.1093/bioinformatics/btu393

Herrera-Estrada, J. E., Martinez, J. A., Dominguez, F., Findell, K. L., Wood, E. F., & Sheffield, J. (2019). Reduced moisture transport linked to drought propagation across North America. *Geophysical Research Letters*, *46*, 5243–5253. https://doi.org/10.1029/2019GL082475

Jaramillo, F., & Destouni, G. (2015). Local flow regulation and irrigation raise global human water consumption and footprint. *Science*, *350*(6265), 1248–1251. https://doi.org/10.1126/science.aad1010

Keune, J., & Miralles, D. G. (2019). A precipitation recycling network to assess the vulnerability of freshwater: challenging the watershed convention (DATA). Figshare. Dataset. https://doi.org/10.6084/m9.figshare.9725084.v1

Keune, J., Sulis, M., Kollet, S., Siebert, S., & Wada, Y. (2018). Human water use impacts on the strength of the continental sink for atmospheric water. *Geophysical Research Letters*, *45*, 4068–4076. https://doi.org/10.1029/2018GL077621

Keys, P. W., Barnes, E. A., Van der Ent, R. J., & Gordon, L. J. (2014). Variability of moisture recycling using a precipitationshed framework. *Hydrology and Earth System Sciences*, *18*(10), 3937–3950. https://doi.org/10.5194/hess-18-3937-2014

Keys, P. W., Van der Ent, R. J., Gordon, L. J., Hoff, H., Nikoli, R., & Savenije, H. H. G. (2012). Analyzing precipitationsheds to understand the vulnerability of rainfall dependent regions. *Biogeosciences*, *9*(2), 733–746. https://doi.org/10.5194/bg-9-733-2012

Keys, P. W., Wang-Erlandsson, L., & Gordon, L. J. (2018). Megacity precipitationsheds reveal tele-connected water security challenges. *PLoS ONE*, *13*(3), e0194311. https://doi.org/10.1371/journal.pone.0194311

Keys, P. W., Wang-Erlandsson, L., Gordon, L. J., Galaz, V., & Ebbesson, J. (2017). Approaching moisture recycling governance. *Global Environmental Change*, *45*, 15–23. https://doi.org/10.1016/j.gloenvcha.2017.04.007

Koster, R. D., Dirmeyer, P. A., Guo, Z., Bonan, G., Chan, E., Cox, P., et al. (2004). Regions of strong coupling between soil moisture and precipitation. *Science*, *305*(5687), 1138–1140. https://doi.org/10.1126/science.1100217

Kummu, M., Guillaume, J. H. A., de Moel, H., Eisner, S., Flörke, M., Porkka, M., et al. (2016). The world's road to water scarcity: Shortage and stress in the 20th century and pathways towards sustainability. *Scientific Reports*, *6*(1), 38,495. https://doi.org/10.1038/srep38495

Kummu, M., Ward, P. J., de Moel, H., & Varis, O. (2010). Is physical water scarcity a new phenomenon? Global assessment of water shortage over the last two millennia. *Environmental Research Letters*, *5*(3), 034006. https://doi.org/10.1088/1748-9326/5/3/034006

Lehner, B., Verdin, K., & Jarvis, A. (2006). HydroSHEDS technical documentation, version 1.0. World Wildlife Fund US, Washington, DC, 1-27.

Liu, J., Yang, H., Gosling, S. N., Kummu, M., Flörke, M., Pfister, S., et al. (2017). Water scarcity assessments in the past, present, and future. *Earth's Future*, *5*(6), 545–559. https://doi.org/10.1002/2016EF000518

Martens, B., Miralles, D. G., Lievens, H., van der Schalie, R., de Jeu, R. A. M., Fernández-Prieto, D., et al. (2017). GLEAM v3: Satellite-based land evaporation and root-zone soil moisture. *Geoscientific Model Development*, *10*(5), 1903–1925. https://doi.org/10.5194/gmd-10-1903-2017

McDonald, R. I., Green, P., Balk, D., Fekete, B. M., Revenga, C., Todd, M., & Montgomery, M. (2011). Urban growth, climate change, and freshwater availability. *Proceedings of the National Academy of Sciences*, *108*(15), 6312–6317. https://doi.org/10.1073/pnas.1011615108

Mekonnen, M. M., & Hoekstra, A. Y. (2016). Four billion people facing severe water scarcity. *Science Advances*, *2*(2), e1500323. https://doi.org/10.1126/sciadv.1500323

Miralles, D. G., De Jeu, R. A. M., Gash, J. H., Holmes, T. R. H., & Dolman, A. J. (2011). An application of GLEAM to estimating global evaporation. *Hydrology and Earth System Sciences Discussions*, *8*(1). https://doi.org/10.5194/gmd-10-1903-2017

Miralles, D. G., Gentine, P., Seneviratne, S. I., & Teuling, A. J. (2019). Land–atmospheric feedbacks during droughts and heatwaves: State of the science and current challenges. *Annals of the New York Academy of Sciences*, *1436*(1), 19–35. https://doi.org/10.1111/nyas.13912

Miralles, D. G., Nieto, R., McDowell, N. G., Dorigo, W. A., Verhoest, N. E., Liu, Y., et al. (2016). Contribution of water-limited ecoregions to their own supply of rainfall. *Environmental Research Letters*, *11*(12), 124007. https://doi.org/10.1088/1748-9326/11/12/124007

Nieto, R., Gimeno, L., & Trigo, R. M. (2006). A Lagrangian identification of major sources of Sahel moisture. *Geophysical Research Letters*, *33*, L18707. https://doi.org/10.1029/2006GL027232

Oki, T., & Kanae, S. (2006). Global hydrological cycles and world water resources. *Science*, *313*(5790), 1068–1072. https://doi.org/10.1126/science.1128845

Orth, R., & Destouni, G. (2018). Drought reduces blue-water fluxes more strongly than green-water fluxes in Europe. *Nature Communications*, *9*(1), 3602. https://doi.org/10.1038/s41467-018-06013-7

Orth, R., Zscheischler, J., & Seneviratne, S. I. (2016). Record dry summer in 2015 challenges precipitation projections in Central Europe. *Scientific Reports*, *6*, 28,334. https://doi.org/10.1038/srep28334

Padowski, J. C., Gorelick, S. M., Thompson, B. H., Rozelle, S., & Fendorf, S. (2015). Assessment of human–natural system characteristics influencing global freshwater supply vulnerability. *Environmental Research Letters*, *10*(10). https://doi.org/10.1088/1748-9326/10/10/104014

Pisso, I., Marécal, V., Legras, B., & Berthet, G. (2010). Sensitivity of ensemble Lagrangian reconstructions to assimilated wind time step resolution. *Atmospheric Chemistry and Physics*, *10*(7), 3155–3162. https://doi.org/10.5194/acp-10-3155-2010

Postel, S. L. (2000). Entering an era of water scarcity: The challenges ahead. *Ecological Applications*, *10*(4), 941–948. https://doi.org/10.1890/1051-0761(2000)010[0941:EAEOWS]2.0.CO;2

Ramos, A. M., Blamey, R. C., Algarra, I., Nieto, R., Gimeno, L., Tomé, R., et al. (2019). From Amazonia to southern Africa: Atmospheric moisture transport through low-level jets and atmospheric rivers. *Annals of the New York Academy of Sciences*, *1436*(1), 217–230. https://doi.org/10.1111/nyas.13960

Rijsberman, F. R. (2006). Water scarcity: Fact or fiction? *Agricultural Water Management*, *80*(1-3), 5–22. https://doi.org/10.1016/j.agwat.2005.07.001

Rockström, J., Falkenmark, M., Karlberg, L., Hoff, H., Rost, S., & Gerten, D. (2009). Future water availability for global food production: The potential of green water for increasing resilience to global change. *Water Resources Research*, *45*, W00A12. https://doi.org/10.1029/2007WR006767

Rodell, M., Famiglietti, J. S., Wiese, D. N., Reager, J. T., Beaudoing, H. K., Landerer, F. W., & Lo, M. H. (2018). Emerging trends in global freshwater availability. *Nature*, *557*(7707), 651–659. https://doi.org/10.1038/s41586-018-0123-1

Schär, C., Lüthi, D., Beyerle, U., & Heise, E. (1999). The soil–precipitation feedback: A process study with a regional climate model. *Journal of Climate*, *12*(3), 722–741. https://doi.org/10.1175/1520-0442(1999)012<0722:TSPFAP>2.0.CO;2

Schewe, J., Heinke, J., Gerten, D., Haddeland, I., Arnell, N. W., Clark, D. B., et al. (2014). Multimodel assessment of water scarcity under climate change. *Proceedings of the National Academy of Sciences*, *111*(9), 3245–3250. https://doi.org/10.1073/pnas.1222460110

Schumacher, D. L., Keune, J., Van Heerwaarden, C. C., Vilà-Guerau De Arellano, J., Teuling, A. J., & Miralles, D. G. (2019). Amplification of mega-heatwaves through heat torrents fuelled by upwind drought. *Nature Geoscience*, *12*(9), 712–717. https://doi.org/10.1038/s41561-019-0431-6

Seneviratne, S. I., Corti, T., Davin, E. L., Hirschi, M., Jaeger, E. B., Lehner, I., et al. (2010). Investigating soil moisture–climate interactions in a changing climate: A review. *Earth-Science Reviews*, *99*(3-4), 125–161. https://doi.org/10.1016/j.earscirev.2010.02.004

Sheffield, J., & Wood, E. F. (2008). Projected changes in drought occurrence under future global warming from multi-model, multi-scenario, IPCC AR4 simulations. *Climate Dynamics*, *31*(1), 79–105. https://doi.org/10.1007/s00382-007-0340-z

Sodemann, H., Schwierz, C., & Wernli, H. (2008). Interannual variability of Greenland winter precipitation sources: Lagrangian moisture diagnostic and North Atlantic Oscillation influence. *Journal of Geophysical Research*, *113*, D03107. https://doi.org/10.1029/2007JD008503

Stohl, A. (1998). Computation, accuracy and applications of trajectories—A review and bibliography. *Atmospheric Environment*, *32*(6), 947–966. https://doi.org/10.1016/S1352-2310(97)00457-3

Stohl, A., Forster, C., Frank, A., Seibert, P., & Wotawa, G. (2005). The Lagrangian particle dispersion model FLEXPART version 6.2. *Atmospheric Chemistry and Physics*, *5*(9), 2461–2474. https://doi.org/10.5194/acp-5-2461-2005

Stohl, A., Forster, C., & Sodemann, H. (2008). Remote sources of water vapor forming precipitation on the Norwegian west coast at 60 N—A tale of hurricanes and an atmospheric river. *Journal of Geophysical Research*, *113*, D05102. https://doi.org/10.1029/2007JD009006

Stohl, A., & James, P. (2004). A Lagrangian analysis of the atmospheric branch of the global water cycle. Part I: Method description, validation, and demonstration for the August 2002 flooding in central Europe. *Journal of Hydrometeorology*, *5*(4), 656–678. https://doi.org/10.1175/1525-7541(2004)005<0656:ALAOTA>2.0.CO;2

Trenberth, K. E. (1999). Atmospheric moisture recycling: Role of advection and local evaporation. *Journal of Climate*, *12*(5), 1368–1381. https://doi.org/10.1175/1520-0442(1999)012<1368:AMRROA>2.0.CO;2

United Nations (2015). Transforming our world: The 2030 agenda for sustainable development. Resolution adopted by the General Assembly on 25 September 2015. A RES/70/1.

Van der Ent, R. J., Savenije, H. H., Schaefli, B., & Steele-Dunne, S. C. (2010). Origin and fate of atmospheric moisture over continents. *Water Resources Research*, *46*, W09525. https://doi.org/10.1029/2010WR009127

Van der Ent, R. J., & Savenije, H. H. G. (2011). Length and time scales of atmospheric moisture recycling. *Atmospheric Chemistry and Physics*, *11*(5), 1853–1863. https://doi.org/10.5194/acp-11-1853-2011

Van der Ent, R. J., & Tuinenburg, O. A. (2017). The residence time of water in the atmosphere revisited. *Hydrology and Earth System Sciences*, *21*(2), 779–790. https://doi.org/10.5194/hess-21-779-2017

Vanham, D., & Bidoglio, G. (2013). A review on the indicator water footprint for the EU28. *Ecological Indicators*, *26*, 61–75. https://doi.org/10.1016/j.ecolind.2012.10.021

Veldkamp, T. I. E., Wada, Y., Aerts, J. C. J. H., & Ward, P. J. (2016). Towards a global water scarcity risk assessment framework: Incorporation of probability distributions and hydro-climatic variability. *Environmental Research Letters*, *11*(2), 024006. https://doi.org/10.1088/1748-9326/11/2/024006

Vicente-Serrano, S. M., Beguería, S., & López-Moreno, J. I. (2010). A multiscalar drought index sensitive to global warming: The standardized precipitation evapotranspiration index. *Journal of Climate*, *23*(7), 1696–1718. https://doi.org/10.1175/2009JCLI2909.1

Vörösmarty, C. J., Green, P., Salisbury, J., & Lammers, R. B. (2000). Global water resources: Vulnerability from climate change and population growth. *Science*, *289*(5477), 284–288. https://doi.org/10.1126/science.289.5477.284

Vörösmarty, C. J., Hoekstra, A. Y., Bunn, S. E., Conway, D., & Gupta, J. (2015). What scale for water governance. *Science*, *349*(6247), 478–479. https://doi.org/10.1126/science.349.6247.478-a

Vörösmarty, C. J., McIntyre, P. B., Gessner, M. O., Dudgeon, D., Prusevich, A., Green, P., et al. (2010). Global threats to human water security and river biodiversity. *Nature*, *468*(7321), 334–561. https://doi.org/10.1038/nature09549

Wang-Erlandsson, L., Fetzer, I., Keys, P. W., van Der Ent, R. J., Savenije, H. H., & Gordon, L. J. (2018). Remote land use impacts on river flows through atmospheric teleconnections. *Hydrology and Earth System Sciences*, *22*(8), 4311–4328. https://doi.org/10.5194/hess-22-4311-2018

Wheater, H. S. (2015). Water security—Science and management challenges. *Proceedings of the International Association of Hydrological Sciences*, *366*, 23–30. https://doi.org/10.5194/piahs-366-23-2015

Winschall, A., Sodemann, H., Pfahl, S., & Wernli, H. (2014). How important is intensified evaporation for Mediterranean precipitation extremes? *Journal of Geophysical Research: Atmospheres*, *119*, 5240–5256. https://doi.org/10.1002/2013JD021175

Young, G., Demuth, S., Mishra, A., & Cudennec, C. (2015). Hydrological sciences and water security: An overview. *Proceedings of the International Association of Hydrological Sciences*, *366*, 1–9. https://doi.org/10.5194/piahs-366-1-2015

Zemp, D. C., Schleussner, C. F., Barbosa, H. M., Hirota, M., Montade, V., Sampaio, G., et al. (2017). Self-amplified Amazon forest loss due to vegetation-atmosphere feedbacks. *Nature Communications*, *8*, 14,681. https://dx.doi.org/10.1038/ncomms14681